Research article

Carbon Future

Dielectric-mediated interfacial ion transport enabling stable lithium metal batteries

Shuoqing Zhang[1,2], Haotian Zhu[2], Junyi Hua[2], Jinze Wang[2,3], Long Li[2], Long Chen[2,3], Ruhong Li[2,3], Lixin Chen[2,4], Xiulin Fan[2]✉, and Tao Deng[1]✉

[1] *China-UK Low Carbon College, Shanghai Jiao Tong University, Shanghai 201306, China*
[2] *State Key Laboratory of Silicon and Advanced Semiconductor Materials, School of Materials Science and Engineering, Zhejiang University, Hangzhou 310027, China*
[3] *ZJU-Hangzhou Global Scientific and Technological Innovation Center, Zhejiang University, Hangzhou 311215, China*
[4] *Key Laboratory of Hydrogen Storage and Transportation Technology of Zhejiang Province, Hangzhou 310027, China*

Cite This: *Carbon Future* **2026**, *3*, 9200068

Read Online

ABSTRACT: Unregulated interfacial electric fields critically undermine the stability of lithium-metal batteries (LMBs) by driving heterogeneous Li^+ flux and dendritic deposition. Here, we report a dielectric-mediated electrolyte design that actively modulates the local electric field to enable uniform Li^+ transport and Li^0 deposition. By integrating fluorinated diluents with varying dielectric constants into localized high-concentration electrolytes (LHCE), a stable dielectric environment was constructed at the Li–electrolyte interface. Specifically, the high-dielectric diluent 1,1,1,3,3-pentafluorobutane facilitates electrolyte to realize uniform and flat lithium deposition under high current density of 3 $mA·cm^{-2}$ by suppressing the electrostatic tip effect that typically triggers dendrite formation. The optimized electrolyte achieves high Coulombic efficiency (> 99.5%), negligible growth in interfacial impedance, and stable cycling in thin Li-based cells. Moreover, Li (30 μm)||$LiCoO_2$ (3.6 $mAh·cm^{-2}$) full cells retain 80% of their initial capacity after 250 cycles within a voltage window of 3–4.5 V, outperforming the reference cells (< 50 cycles) using high-concentration electrolyte and LHCE with low-dielectric-constant diluent. The strategy of dielectric-mediated interface homogenizes electric field distribution and stabilizes ion transport beyond conventional interphase-focused approaches. This work establishes dielectric modulation as a viable paradigm for interfacial regulation, advancing the design of high-energy-density LMBs.

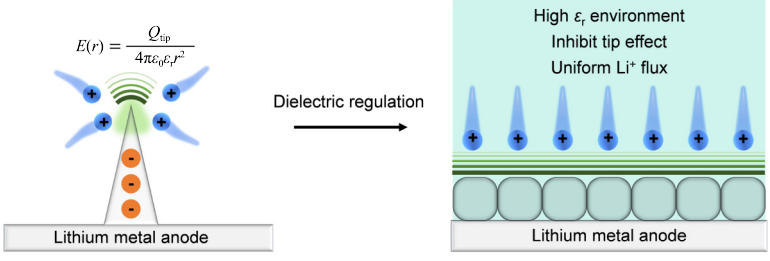

KEYWORDS: lithium metal anode, dielectric regulation, ion transport, electrolyte engineering, lithium battery

1 Introduction

Lithium-metal batteries (LMBs) are considered a promising solution to fulfill the growing demand for high-energy-density systems, particularly in achieving cell-level specific energies exceeding 350–500 $Wh·kg^{-1}$ [1–6]. However, LMBs face persistent interfacial instabilities at the lithium metal/electrolyte interface, including the continuous formation and fracture nature of the solid-electrolyte interphase (SEI), as well as the growth of dendritic lithium deposits[7–9]. These issues collectively lead to degraded Coulombic efficiency (CE), shortened cycle life, and compromised safety. The pursuit of advanced LMBs has spurred extensive research into electrolyte engineering[10–17], aiming to protect the lithium metal anode (LMA) by forming a stable SEI[18–20]. Nevertheless, beyond SEI stabilization, the Li plating process, particularly the reduction of Li^+ to Li^0, is also governed by the intrinsic electric field at the electrode/electrolyte interface[21–23]. Notably, this interfacial electric field evolves dynamically in response to real-time charge–discharge protocols, and Li^+ flow also varies accordingly. Unregulated Li^+ migration behavior under such dynamically changing electric fields remains a significant impediment to the practical deployment of LMBs, particularly under realistic operational conditions with limited available LMA capacity.

A key origin of the morphological instability during Li plating is the classical electrostatic "tip effect": Local protrusions or surface asperities concentrate excess charge, leading to an intensified electric field at their apexes, which enhances Li^+ attraction and directs Li^0 preferentially toward these sites[24, 25]. Such selective Li deposition amplifies initial microscopic roughness into ramified dendrites and isolated "dead Li". Both theoretical analyses and *operando* imaging studies have identified localized charge

Received: November 28, 2025; **Revised:** January 19, 2026
Accepted: February 7, 2026

✉Address correspondence to Xiulin Fan, xlfan@zju.edu.cn; Tao Deng, taodeng@sjtu.edu.cn

https://doi.org/10.26599/CF.2026.9200068

accumulation and heterogeneous Li^+ flux near protrusions as key contributors to the failure of LMBs. Given this mechanistic picture, suppressing the tip effect necessitates deliberate modulation of the local interfacial electric field to redistribute ionic flux. Electrolyte engineering using non-lithium cationic additives has yielded promising laboratory demonstrations of more uniform Li plating[22, 23, 26, 27]. These cationic additives are intended to preferentially occupy high-electric-field regions, thereby steering deposition toward flatter areas. However, such strategies are mainly effective during the Li plating step and often fail to maintain effectiveness during the subsequent stripping process. Therefore, effective suppression of the tip effect requires strategies that function reliably throughout both Li plating and stripping in round-trip processes.

To address the aforementioned challenges, we propose a dielectric-mediated strategy that directly modulates the interfacial electric field governing Li^+ migration. This concept is implemented by using localized high-concentration electrolytes (LHCE) incorporating fluorinated diluents with distinct dielectric properties, thereby enabling the formation of stable interfacial dielectric layers. A flat and dense Li deposition morphology can be achieved under high current density conditions in LHCE with a high-dielectric environment. Systematic analysis reveals that incorporating a high-dielectric diluent enhances interfacial capacitance, accelerates Li^+ diffusion kinetics, and enables stable cycling of high-voltage LMBs.

2 Results and discussion

2.1 Modulating interfacial lithium-ion diffusion through dielectric screening

To mitigate the tip effect on lithium metal surfaces, it is essential to elucidate its origin and establish a quantitative description. As illustrated in **Fig. 1a**, the charge accumulated at a Li protrusion, denoted as Q_{tip}, generates a localized electric field in its vicinity. The strength of this field can be expressed as a function of the spatial coordinate r

$$E(r) = \frac{Q_{tip}}{4\pi\varepsilon_0\varepsilon_r r^2} \quad (1)$$

where ε_0 represents the vacuum permittivity and ε_r represents the relative dielectric constant of the surrounding medium. Under this field, Li ions experience an attractive Coulombic force toward the tip, where they are subsequently reduced to metallic Li^0, driving the rapid growth of dendritic structures. The Coulombic force acting on a Li^+ at a distance r from the field center can thus be described as

$$F = q_+ \times E(r) = \frac{Q_{tip} \times q_+}{4\varepsilon_0\varepsilon_r r^2} \quad (2)$$

where q_+ represents the charge of a Li^+ (Fig. 1b). To suppress the tip effect, the attractive force exerted on Li^+ within the interfacial field must be reduced. As evident from Eq. (2) and Fig. 1c, the magnitude of the Coulombic force F strongly depends on the dielectric environment at the Li tip. A higher dielectric constant effectively shields the local electric field, diminishing the directional migration of Li^+ toward the protrusion, thereby promoting more uniform Li deposition. Consequently, the potential distribution on a planar Li surface becomes more homogeneous, eliminating localized field intensification and stabilizing interfacial ion transport (Fig. 1d). Thus, tailoring the dielectric environment at the Li–electrolyte interface provides a feasible way to suppress the tip effect. Notably, unlike cation-selective adsorption strategies, this dielectric regulation approach constructs a persistent interfacial dielectric environment that remains operative throughout both Li plating and stripping processes.

To implement the above dielectric modulation strategy through electrolyte engineering, we adopted the LHCE concept, which offers

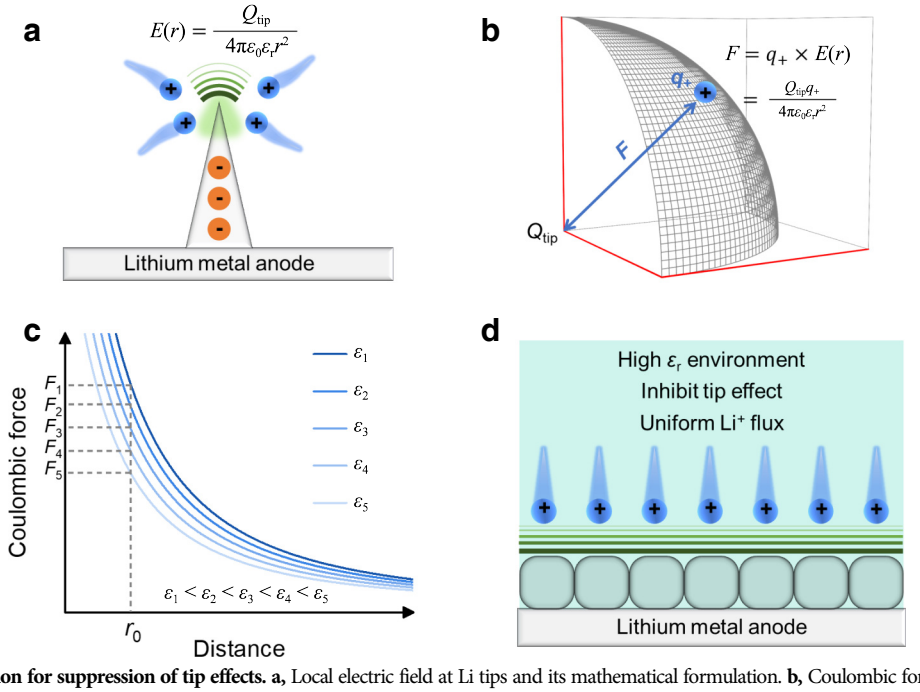

Fig. 1. Dielectric regulation for suppression of tip effects. a, Local electric field at Li tips and its mathematical formulation. **b,** Coulombic force exerted on a Li^+ at any given position within the electric field generated by Q_{tip}. **c,** Relationship between Coulombic forces and the dielectric environment. **d,** Homogeneous interfacial ion transport and deposition enabled by dielectric modulation.

high compositional tunability (Supplementary Fig. S1). In such electrolytes, the lithium salt and solvent form the primary solvation structure that dictates the physicochemical properties of the system. The diluent, as an inert co-solvent, further refines this solvation structure[28], enabling improved electrochemical performance. Consequently, an LHCE can be regarded as solvated Li^+ complexes dispersed within a dielectric medium provided by the diluent. This configuration allows the dielectric environment surrounding the solvation structure to be tuned via the dielectric properties of the diluent, thereby regulating interfacial reaction conditions. Here, we employed a 10 m solution of lithium bis(fluorosulfonyl)imide (LiFSI) in 1,2-dimethoxyethane (DME) solvent as the 10 m LiFSI-DME baseline electrolyte (denoted as FD), which features anion-involved coordination in the Li^+ solvation sheath (Supplementary Fig. S2), ensuring both reductive stability toward Li metal and oxidative stability at high-voltage cathodes. Two diluents (1,1,2,2,3,3,4-heptafluorocyclopentane (HFCP) and 1,1,1,3,3-pentafluorobutane (PFB)) with distinct dielectric constants (2.1 and 11.99, respectively) were then introduced to modulate the solvation environment, yielding 10 m LiFSI-DME-HFCP electrolyte (denoted as FDH) and 10 m LiFSI-DME-PFB electrolyte (denoted as FDP), respectively.

2.2 Investigation of Li plating/stripping reversibility and behavior

To validate the practical effectiveness of the dielectric modulation strategy, we evaluated the Li plating/stripping behavior using FD, FDH, and FDP electrolytes. To better represent the realistic LMB conditions, thin Li foils (30 μm, denoted Li30) were used instead of conventional thick Li foils (450 μm). As shown in **Fig. 2a**, the consumption of active Li during cycling was monitored in Li30||Cu cells. In the FD and FDH electrolytes, the cell voltage begins to fluctuate at an early stage and eventually reaches the cut-off voltage (1 V), indicating cell failure. In contrast, the FDP electrolyte enables much more stable Li plating/stripping over extended cycles. The reversibility of Li plating/stripping was further assessed by the CE values (Fig. 2b). Compared with FD, both FDH and FDP electrolytes exhibit a rapid increase in CE to 99.5%, owing to the improved physicochemical properties imparted by the diluents. Nevertheless, FDP delivers a markedly longer cycling lifespan (> 50 cycles) than FDH (< 40 cycles). This high reversibility arises from fewer electrons being consumed during the irreversible SEI formation stage, resulting in more efficient passivation of the Cu surface. This inference is corroborated by the shorter time required for the Cu electrode potential to drop to zero in the FDP electrolyte (Fig. 2c), reflecting faster and more complete interfacial stabilization.

Furthermore, the cycling stability of symmetric Li30||Li30 cells was evaluated in the three electrolytes at the condition of 1 $mA{\cdot}cm^{-2}$ and 4 $mAh{\cdot}cm^{-2}$ (Fig. 2d). The cycle lifespan follows the order of FD < FDH < FDP, a trend that persists even under a higher current density (Supplementary Fig. S3). Notably, in the FDP electrolyte, the interfacial impedance of the Li30||Li30 cells exhibits negligible growth over prolonged cycling (Fig. 2e), whereas significant impedance increases are observed in both FD and FDH systems (Supplementary Fig. S4). This indicates that the SEI formed in FDP effectively suppresses continuous parasitic reactions between Li metal and the electrolyte, thereby maintaining interfacial integrity.

To further probe Li corrosion behavior, Li was first deposited onto the Cu substrate and then aged for seven days before testing the plating/stripping reversibility (Supplementary Fig. S5). As shown in Fig. 2f, the FDP electrolyte delivers not only a high 2nd cycle CE of 99.49% but also retains the highest CE value (98.28%) after aging among the three electrolytes. The above results collectively demonstrate that FDP electrolyte not only facilitates the formation of a stable SEI to ensure consistent cycling performance of LMA, but also mitigates Li corrosion during long-term operation. Additionally, the dielectric environment established by PFB contributes to more stable Li plating/stripping dynamics while

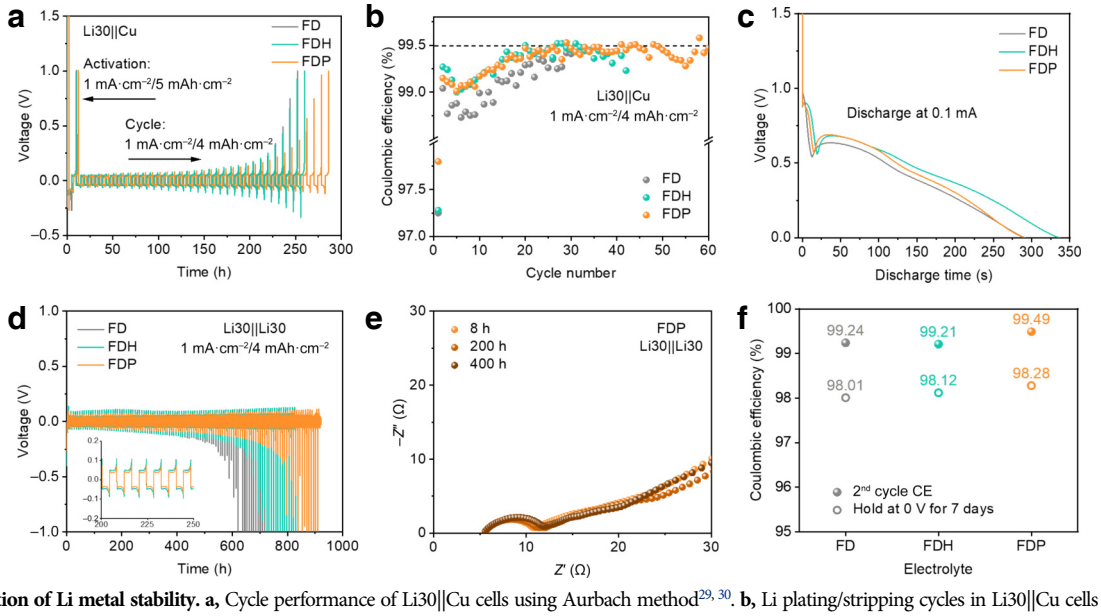

Fig. 2. Evaluation of Li metal stability. a, Cycle performance of Li30||Cu cells using Aurbach method[29, 30]. **b,** Li plating/stripping cycles in Li30||Cu cells at 1 $mA{\cdot}cm^{-2}$ with a fixed capacity of 4 $mAh{\cdot}cm^{-2}$. **c,** Voltage–time curve of Li30||Cu cells discharging to 0 V at 0.1 mA. **d,** Cycle tests of Li30||Li30 cells at 1 $mA{\cdot}cm^{-2}$ with a fixed capacity of 4 $mAh{\cdot}cm^{-2}$. **e,** Electrochemical impedance spectra (EIS) plot of Li30||Li30 cells after cycling for different durations. **f,** CE values of Li30||Cu cells before and after aging for seven days.

suppressing Li dendrite growth and dead Li accumulation over prolonged cycling.

To elucidate the impact of dielectric modulation on Li deposition, we investigated the Li plating behavior across three electrolytes under varying current densities. As the tip effect during metal deposition intensifies with the increase of current density, we compared the morphological evolution of Li deposits accordingly (**Figs. 3**a–3i). Quantitative analysis was conducted by evaluating the variation of the average deposit area with current density in different electrolytes (Fig. 3j and Supplementary Fig. S6). In the FD electrolyte, the average deposit area remains nearly constant (21.52 and 22.88 μm^2) at 1 and 2 mA·cm^{-2} but declines sharply at 3 mA·cm^{-2} (11.32 μm^2). This reduction stems from the sluggish Li^+ transport in FD (Supplementary Figs. S7 and S8), which elevates the overpotential at high current densities, promotes excessive nucleation, and consequently yields smaller deposits[31]. In the FDH electrolyte, the deposit area is larger (40.40 μm^2) at 1 mA·cm^{-2} but decreased drastically to 15.74 and 13.14 μm^2 at 2 and 3 mA·cm^{-2}, respectively. The relatively rapid Li^+ diffusion in FDH supports deposition at a low rate but becomes inadequate at high rates (Supplementary Figs. S7 and S8). Moreover, the low dielectric constant of HFCP provides limited mitigation of the tip effect, resulting in the formation of numerous small Li clusters. In contrast, the FDP electrolyte exhibits negligible variation in average deposit areas (23.51, 20.50, and 20.37 μm^2) with increasing current density, reflecting both its superior Li^+ diffusivity and strong suppression of the tip effect imparted by the high dielectric constant of PFB. This synergy enables stable and uniform Li deposition across a wide current range. Furthermore, the evolution of deposit thickness can also highlight the role of dielectric modulation (Fig. 3k and Supplementary Fig. S9). Owing to the low ionic conductivity of FD, Li deposition at high current densities is prematurely terminated by cut-off voltage, leading to reduced deposit thickness. In FDH and FDP, however, the Li deposit thickness increases with current density, indicative of more porous growth. Notably, the thickness in FDP approaches the theoretical value, suggesting that the dielectric shielding of PFB redistributes the local electric field, facilitating lithium diffusion toward non-tip regions and promoting denser deposition.

The nitrogen content on deposited Li surfaces was further analyzed to assess the contribution of anion decomposition to SEI formation (Fig. 3l). These nitrogen-containing species mainly correspond to LiFSI, Li_3N, and the intermediate N-SO_x products from the decomposition of the FSI anion[32]. Acting as SEI components with high ionic conductivity, they facilitate Li ion transport across the interface, enabling uniform Li deposition[33]. Compared to FD and FDH, higher nitrogen levels are detected in the FDP electrolyte, indicating enhanced anion decomposition and the formation of an inorganic-rich SEI. The mechanically robust SEI thus formed effectively inhibits dendritic growth. Therefore, the FDP electrolyte simultaneously suppresses the tip effect through the high dielectric constant of PFB and promotes the construction of a mechanically reinforced, inorganic-rich SEI via enhanced anion decomposition, thereby achieving uniform and dendrite-free Li deposition.

2.3 Impact of diluent properties on the effectiveness of dielectric modulation

Beyond the dielectric constant, both the magnitude and orientation of a molecular dipole moment govern its responsiveness to external electric fields (**Figs. 4**a and 4b). PFB exhibits a larger dipole moment (4.18 D) than HFCP (2.89 D), suggesting that PFB is more sensitive to interfacial electric fields and can more effectively modulate the local dielectric environment (Fig. 4c). To substantiate this, we measured the interfacial electric double-layer capacitance

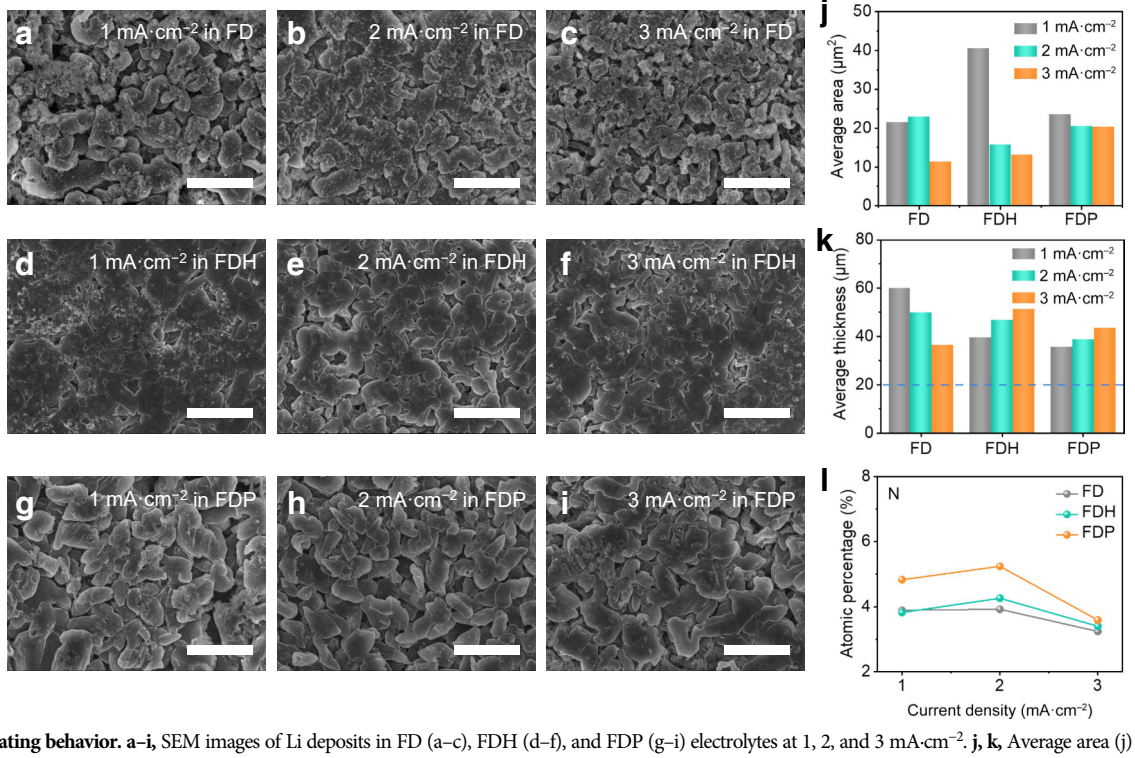

Fig. 3. Li plating behavior. a–i, SEM images of Li deposits in FD (a–c), FDH (d–f), and FDP (g–i) electrolytes at 1, 2, and 3 mA·cm^{-2}. **j, k,** Average area (j) and average thickness (k) of Li deposits. **l,** Atomic percentage in SEI components on Li metal surface.

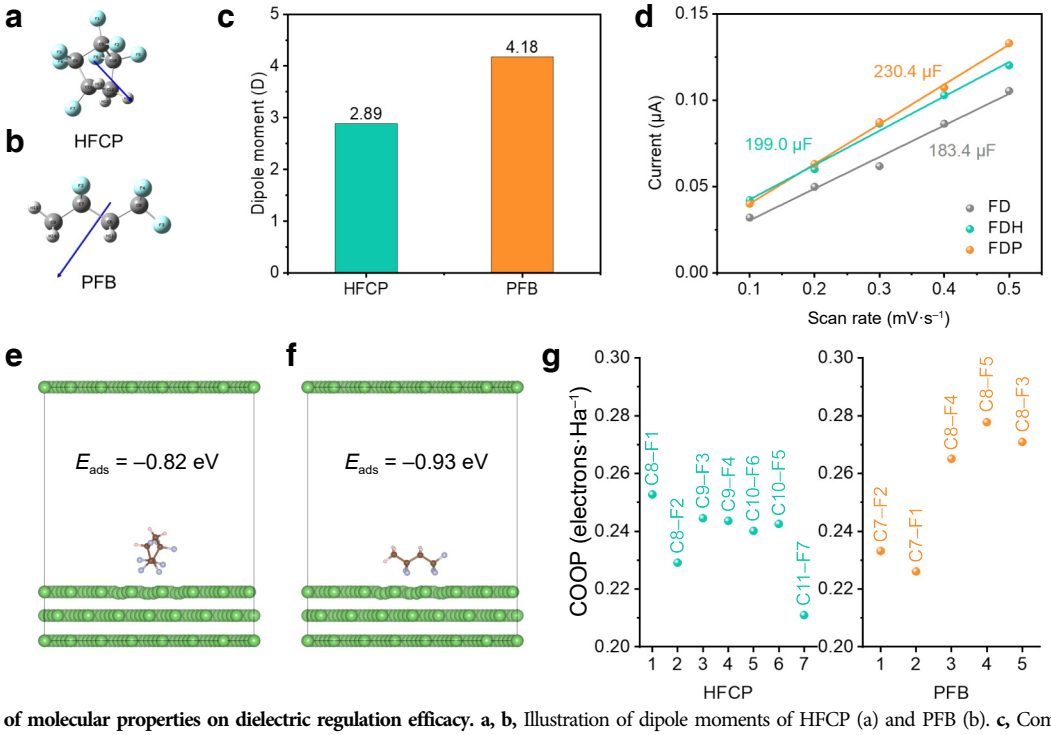

Fig. 4. Influence of molecular properties on dielectric regulation efficacy. a, b, Illustration of dipole moments of HFCP (a) and PFB (b). **c,** Comparison of dipole moments. **d,** Interfacial C_{dl} in diverse electrolytes. **e, f,** Adsorption energies of HFCP (e) and PFB (f) on Li metal. **g,** COOP for different C–F bonds. The atomic numbering scheme is illustrated in Supplementary Fig. S13.

(C_{dl}) for different electrolytes within the non-Faradaic region (Supplementary Figs. S10 and S11). As shown in Fig. 4d, C_{dl} increases sequentially from FD (183.4 μF) to FDH (199.0 μF) and FDP (230.4 μF). This trend indicates that the Li-FDP interface possesses a higher effective dielectric constant, consistent with the equation for capacitance[34]

$$C = \frac{\varepsilon_0 \varepsilon_r A}{d} \quad (3)$$

where A is the overlapping area of two plates and d is the distance between them.

The superior dielectric screening imparted by PFB originates not only from its intrinsic dipole and dielectric constant but also from its stronger adsorption on Li metal (–0.93 eV for PFB vs. –0.82 eV for HFCP, Figs. 4e and 4f), attributed to the more pronounced negative electrostatic potential region in PFB (Supplementary Fig. S12). Additionally, the diluent must maintain sufficient chemical stability to ensure effective performance, which is evaluated by the crystal orbital overlap population (COOP) value. A lower COOP value indicates a bond that is more susceptible to cleavage. The robust C–F bonds in PFB stabilize its molecular configuration at the Li–electrolyte interface, ensuring a persistent dielectric layer. In contrast, the weakest C11–F7 bond (COOP = 0.21 Ha) in HFCP is prone to cleavage (Fig. 4g and Supplementary Fig. S13), undermining molecular integrity and diminishing its dielectric shielding capability over time. Furthermore, to decouple the effects of SEI and dielectric screening on stabilizing LMA, 1,1,2,2-tetrachloroethane (TCL) with a comparable ε_r (8.42) to PFB was selected for the preparation of a 10 m LiFSI-DME-TCL electrolyte (denoted as FDT). The disparity in CE between FDP and FDT is initially pronounced but gradually narrowed over cycle number (Supplementary Fig. S14). This indicates that dielectric shielding primarily functions during the initial stage when the SEI is not yet fully developed. Subsequently, as the SEI forms and stabilizes, it assumes a dominant role in maintaining interfacial stability, thereby enabling the high average CE.

2.4 Assessing electrolyte performance in high-voltage LMBs

To assess the practical applicability of the designed electrolytes in high-voltage LMBs, Li30||$LiCoO_2$ full cells were assembled. Prior to cycling, the oxidative stability of the electrolytes was examined, as a high charge cut-off voltage is critical for fully utilizing the capacity and energy density of $LiCoO_2$. Linear sweep voltammetry (LSV) results confirm that all three electrolytes exhibit oxidative stability beyond 4.0 V (**Fig. 5a**), as evaluated based on a decomposition current of 5 μA·cm^{-2}. To further mimic practical conditions, the oxidative endurance of electrolytes was evaluated in Li30||$LiCoO_2$ under different charge cut-off voltages, with the CE used as an indicator (Supplementary Fig. S15). As shown in Fig. 5b, the CE of all Li30||$LiCoO_2$ cells first increases and then decreases with the increase of cut-off voltage. Among them, the Li30||$LiCoO_2$ cell using FDP achieves the highest CE (99.9%) when the cut-off voltage was elevated to 4.5 V, outperforming both cells using FD (99.12%) and FDH (98.41%). Such superior anodic stability of FDP is highly advantageous for enabling long-life and high-voltage LMBs.

The rate performance of Li30||$LiCoO_2$ cells in different electrolytes was subsequently compared (Fig. 5c). The FD electrolyte, characterized by high viscosity and low ionic conductivity, exhibits a sharp capacity drop at 2 C. The FDH system shows improved rate performance due to reduced viscosity imparted by the addition of HFCP diluent. In contrast, the FDP electrolyte enables outstanding high-rate capability, maintaining a specific capacity exceeding 120 mAh·g^{-1} even at 5 C, which corresponds to 70% of the capacity achieved at 0.5 C. Long-term cycling stability was further examined at a cut-off voltage of 4.5 V

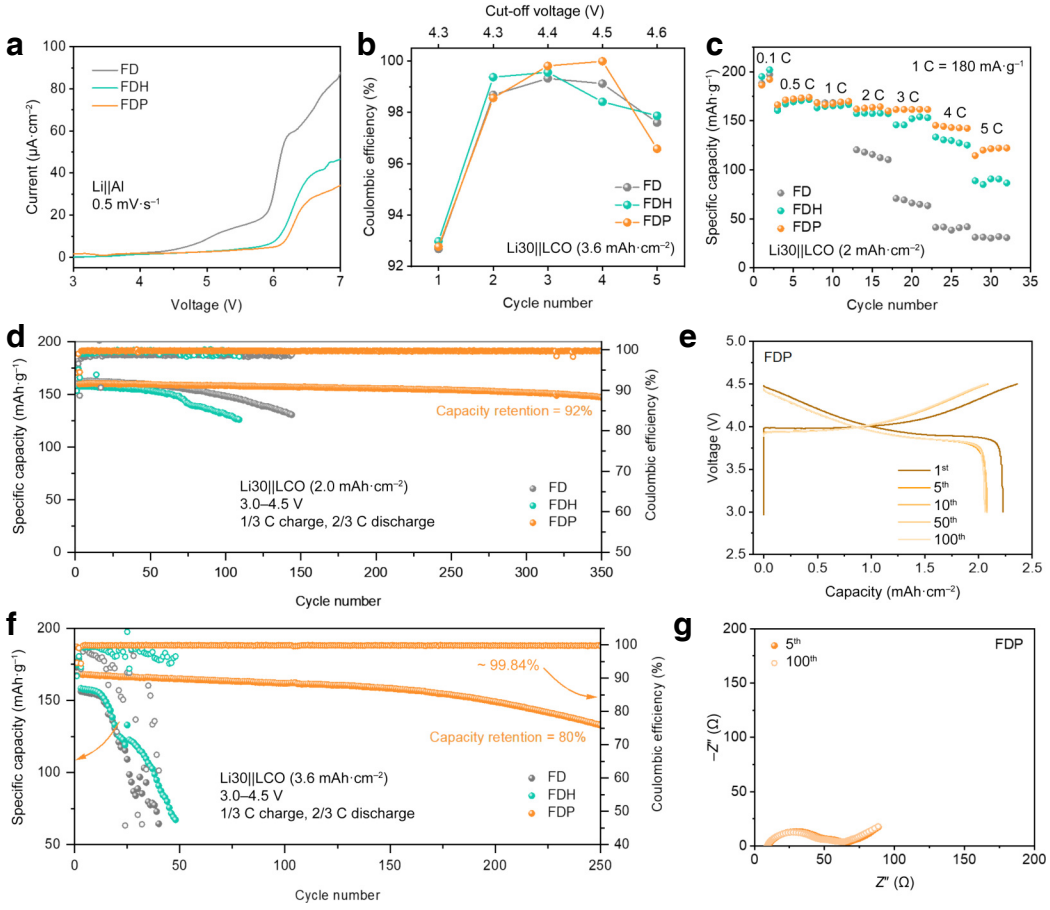

Fig. 5. Electrochemical tests of Li30||$LiCoO_2$ cells. a, LSV plots of Li||Al cells at 0.5 $mV·s^{-1}$. **b,** CE of Li30||$LiCoO_2$ cells as a function of the charge cut-off voltage. **c,** Rate performance of Li30||$LiCoO_2$ cells, 1 C = 180 $mA·g^{-1}$. **d,** Long-term cycle performance of Li30||$LiCoO_2$ cells with a cathode areal loading of 2 $mAh·cm^{-2}$. **e,** Charge/discharge plots of Li30||$LiCoO_2$ cells with FDP. **f,** Cycle performance of Li30||$LiCoO_2$ cells with a cathode areal loading of 3.6 $mAh·cm^{-2}$. **g,** EIS plots of Li30||$LiCoO_2$ cell with FDP after different cycles.

(Fig. 5d). Li30||$LiCoO_2$ cells employing FD and FDH electrolytes suffer from early failure (< 150 cycles), attributed to inferior Li plating/stripping reversibility and limited oxidative stability. By comparison, the FDP-based Li30||$LiCoO_2$ cell retains 92% of its initial capacity after 350 cycles, accompanied by negligible voltage polarization throughout the cycling process (Fig. 5e and Supplementary Fig. S16). When the $LiCoO_2$ areal loading is increased to 3.6 $mAh·cm^{-2}$ (Fig. 5f), cells with FD and FDH electrolytes exhibit rapid capacity degradation, with severe impedance growth within 25 cycles and complete failure after only a few tens of cycles. In contrast, the Li30||$LiCoO_2$ cell incorporating FDP electrolyte sustains stable cycling for over 250 cycles with an 80% capacity retention and an average CE of 99.84%, while maintaining nearly constant interfacial impedance (Fig. 5g and Supplementary Fig. S17).

Collectively, these electrochemical test results underscore that the dielectric environment provided by PFB not only stabilizes Li deposition but also endows the electrolyte with enhanced oxidative robustness and superior interfacial stability, enabling practical high-voltage LMBs.

3 Conclusions

In summary, we demonstrate a dielectric-mediated strategy that effectively stabilizes LMA by tuning interfacial electric fields. Through controlled dielectric screening using high-dielectric and high-dipole fluorinated diluents, local charge accumulation is alleviated, thereby homogenizing Li^+ flux during plating and stripping at high current densities. The high-dielectric PFB diluent forms a persistent dielectric layer that concurrently promotes uniform Li deposition and supports anion-derived SEI formation enriched in inorganic species. As a result, Li||Cu and symmetric Li||Li cells exhibit high Coulombic efficiency (≥ 99.5%), extended lifespan, and suppressed dendritic growth. When paired with high-voltage $LiCoO_2$ cathodes (3.6 $mAh·cm^{-2}$), the electrolyte sustains 4.5 V operation with long-term cycling stability (250 cycles). The dielectric modulation strategy introduced in this study offers a feasible pathway for regulating ion transport dynamics in next-generation rechargeable metal batteries.

References

[1] Huang, H.; Hu, Y. T.; Hou, Y. J.; Wang, X. K.; Dong, Q. J.; Zhao, Z. X.; Ji, M. F.; Zhang, W. X.; Li, J. Y.; Xie, J. P. et al. Delocalized electrolyte design enables 600 $Wh·kg^{-1}$ lithium metal pouch cells. *Nature* **2025**, *644*, 660–667.

[2] Ji, H. J.; Xiang, J. W.; Li, Y.; Zheng, M. T.; Yuan, L. X.; Liao, Y. Q.; Du, L.; Li, Z. Z.; Xie, Z. Y. T.; Huang, K. et al. Liquid–liquid interfacial tension stabilized Li-metal batteries. *Nature* **2025**, *643*, 1255–1262.

[3] Zhang, S. Q.; Li, R. H.; Deng, T.; Ma, Q.; Hong, X.; Zhang, H.; Zhang, R. X.; Ding, S. H.; Wu, Y. J.; Zhu, H. T. et al. Oscillatory

solvation chemistry for a 500 Wh·kg^{-1} Li-metal pouch cell. *Nat. Energy* **2024**, *9*, 1285–1296.

[4] Li, R. H.; Zhang, H. K.; Zhang, S. Q.; Li, Y.; Guo, R.; Pei, H. J.; Yang, M.; Zhang, J. B.; Chen, L.; Xiao, X. Z. et al. Unified affinity paradigm for the rational design of high-efficiency lithium metal electrolytes. *Nat. Energy* **2025**, *10*, 1155–1165.

[5] Xia, Y. C.; Zhou, P.; Kong, X.; Tian, J. K.; Zhang, W. L.; Yan, S. S.; Hou, W. H.; Zhou, H. Y.; Dong, H.; Chen, X. X. et al. Designing an asymmetric ether-like lithium salt to enable fast-cycling high-energy lithium metal batteries. *Nat. Energy* **2023**, *8*, 934–945.

[6] Huang, X. Y.; Zhao, C. Z.; Kong, W. J.; Yao, N.; Shuang, Z. Y.; Xu, P.; Sun, S.; Lu, Y.; Huang, W. Z.; Li, J. L. et al. Tailoring polymer electrolyte solvation for 600 Wh·kg^{-1} lithium batteries. *Nature* **2025**, *646*, 343–350.

[7] Kim, S.; Park, G.; Lee, S. J.; Seo, S.; Ryu, K.; Kim, C. H.; Choi, J. W. Lithium-metal batteries: From fundamental research to industrialization. *Adv. Mater.* **2023**, *35*, 2206625.

[8] Niu, C. J.; Liu, D. Y.; Lochala, J. A.; Anderson, C. S.; Cao, X.; Gross, M. E.; Xu, W.; Zhang, J. G.; Whittingham, M. S.; Xiao, J. et al. Balancing interfacial reactions to achieve long cycle life in high-energy lithium metal batteries. *Nat. Energy* **2021**, *6*, 723–732.

[9] Shadike, Z.; Chen, Y. M.; Liu, L.; Cai, X. Y.; Shen, S. Y.; Zhang, J. L. Improved cyclic stability of $LiNi_{0.8}Mn_{0.1}Co_{0.1}O_2$ cathode enabled by a novel CEI forming additive. *Front. Energy* **2024**, *18*, 535–544.

[10] Wang, H. S.; Yu, Z.; Kong, X.; Kim, S. C.; Boyle, D. T.; Qin, J.; Bao, Z. N.; Cui, Y. Liquid electrolyte: The nexus of practical lithium metal batteries. *Joule* **2022**, *6*, 588–616.

[11] Yang, W. J.; Cai, J. F.; Xu, C. R.; Chen, A. Y.; Wang, Y. G.; Shi, Y. et al. A bipolar solvent molecule design for wide-temperature high-voltage lithium metal batteries. *Adv. Mater.* **2025**, *37*, 2505285.

[12] Jang, J. H.; Wang, C. Z.; Kang, G. M.; Han, C.; Han, J.; Shin, J. S.; Ko, S.; Kim, G.; Baek, J.; Kim, H. T. et al. Miniature Li^+ solvation by symmetric molecular design for practical and safe Li-metal batteries. *Nat. Energy* **2025**, *10*, 502–512.

[13] Yan, S. S.; Liu, H.; Lu, Y.; Feng, Q. Q.; Zhou, H. Y.; Wu, Y. H.; Hou, W. H.; Xia, Y. C.; Zhou, H. Y.; Zhou, P. et al. Selectively fluorinated aromatic lithium salts regulate the solvation structure and interfacial chemistry for all-solid-state batteries. *Sci. Adv.* **2025**, *11*, eads4014.

[14] Xu, Z. X.; Zhang, X. Y.; Yang, J.; Cui, X. X.; Nuli, Y.; Wang, J. L. High-voltage and intrinsically safe electrolytes for Li metal batteries. *Nat. Commun.* **2024**, *15*, 9856.

[15] Ruan, D. G.; Wang, Y. R.; Guo, J. S.; Cui, Z. Z.; Nian, Q. S.; Ma, Z. H.; Wang, D. Z.; Fan, J. J.; Ma, J.; Xiong, B. Q. et al. Oscillating lithium ion-acceptor fluorine-donor electrolytes for practical fast-charging high-energy lithium metal pouch cells. *Energy Environ. Sci.* **2025**, *18*, 6224–6236.

[16] Wang, S.; Zhang, J. Y.; Hua, W. B.; Wen, L. F.; Tang, G. C.; Wang, X.; Ma, C. S.; Chen, W. H. Solvation-enhanced electrolyte on layered oxide cathode tailoring even and stable CEI for durable sodium storage. *Carb. Neutrality* **2023**, *2*, 20.

[17] Huang, J. H.; Feng, Q. K.; Luo, C. Fast Li-ion battery chemistry enabled by small-sized solvent. *Carb. Neutrality* **2024**, *3*, 20.

[18] Zhao, Q.; Stalin, S.; Archer, L. A. Stabilizing metal battery anodes through the design of solid electrolyte interphases. *Joule* **2021**, *5*, 1119–1142.

[19] Xu, Q. S.; Li, T.; Ju, Z. J.; Chen, G. X.; Ye, D. Q.; Waterhouse, G. I. N.; Lu, Y. Y.; Lai, X. J.; Zhou, G. M.; Guo, L. et al. Li_2ZrF_6-based electrolytes for durable lithium metal batteries. *Nature* **2025**, *637*, 339–346.

[20] Xu, K. Interfaces and interphases in batteries. *J. Power Sources* **2023**, *559*, 232652.

[21] Liu, J. X.; Hua, H. M.; Lin, J.; Deng, Y. L.; Pei, N. B.; Zhang, P.; Dong, J. C.; Li, J. F.; Zhao, J. B. Optimizing interface concentration and electric fields for enhanced lithium deposition behavior in lithium metal anodes. *Energy Environ. Sci.* **2024**, *17*, 5993–6002.

[22] Xie, W. X.; Wu, J. X.; Li, X. Y.; Song, Z. G.; Tong, L. J.; Miao, Y. H.; Li, M. X.; Li, X.; Wang, M. X.; Chen, Y. et al. Synergizing interfacial electric field regulation and *in situ* robust interphases for stable lithium metal batteries at high currents. *Angew. Chem.* **2025**, *137*, e202501005.

[23] Ju, Z. Y.; Zheng, T. R.; Marschilok, A. C.; Takeuchi, E. S.; Takeuchi, K. J.; Yu, G. H. Regulating solvation chemistries via electric-field-induced locally concentrated suspension electrolytes for lithium metal batteries. *Adv. Mater.* **2025**, *37*, e08743.

[24] Zou, P. C.; Sui, Y. M.; Zhan, H. C.; Wang, C. Y.; Xin, H. L.; Cheng, H. M.; Kang, F. Y.; Yang, C. Polymorph evolution mechanisms and regulation strategies of lithium metal anode under multiphysical fields. *Chem. Rev.* **2021**, *121*, 5986–6056.

[25] Lin, D. C.; Liu, Y. Y.; Cui, Y. Reviving the lithium metal anode for high-energy batteries. *Nat. Nanotechnol.* **2017**, *12*, 194–206.

[26] Ding, F.; Xu, W.; Graff, G. L.; Zhang, J.; Sushko, M. L.; Chen, X. L.; Shao, Y. Y.; Engelhard, M. H.; Nie, Z. M.; Xiao, J. et al. Dendrite-free lithium deposition via self-healing electrostatic shield mechanism. *J. Am. Chem. Soc.* **2013**, *135*, 4450–4456.

[27] Wang, J. H.; Li, Y. P.; Tu, W. B.; Zhang, H. T.; Yu, X. Y.; Yang, Y. R.; Luo, H. Y.; Zhao, Q. G.; Ru, Y. X.; Chen, M. et al. Regulating dynamic evolution of interfacial electrolyte configuration via inert cation induced anion anchoring to stabilize lithium-metal anode. *Angew. Chem. Int. Ed.* **2025**, *64*, e202513839.

[28] Peng, J. Y.; Zhang, H.; Zeng, Z. Q.; Zhang, H. Y.; Pei, H. J.; Wu, Q.; Shen, Y. B.; Guo, R.; Cheng, S. J.; Xie, J. Tailoring solvation structures via precise diluent engineering for high-rate 500 Wh·kg^{-1} lithium-metal batteries. *Adv. Mater.* **2025**, *37*, e09109.

[29] Adams, B. D.; Zheng, J. M.; Ren, X. D.; Xu, W.; Zhang, J. G. Accurate determination of Coulombic efficiency for lithium metal anodes and lithium metal batteries. *Adv. Energy Mater.* **2018**, *8*, 1702097.

[30] Mohammadi, A.; Djafer, S.; Sayegh, S.; Naylor, A. J.; Bechelany, M.; Younesi, R.; Monconduit, L.; Stievano, L. Assessing Coulombic efficiency in lithium metal anodes. *Chem. Mater.* **2023**, *35*, 2381–2393.

[31] Pei, A.; Zheng, G. Y.; Shi, F. F.; Li, Y. Z.; Cui, Y. Nanoscale nucleation and growth of electrodeposited lithium metal. *Nano Lett.* **2017**, *17*, 1132–1139.

[32] Yu, W. L.; Lin, K. Y.; Boyle, D. T.; Tang, M. T.; Cui, Y.; Chen, Y. L.; Yu, Z. A.; Xu, R.; Lin, Y. J.; Feng, G. X. et al. Electrochemical formation of bis(fluorosulfonyl)imide-derived solid–electrolyte interphase at Li-metal potential. *Nat. Chem.* **2025**, *17*, 246–255.

[33] Zhang, S. Q.; Li, R. H.; Hu, N.; Deng, T.; Weng, S. T.; Wu, Z. C.; Lu, D.; Zhang, H. K.; Zhang, J. B.; Wang, X. F. et al. Tackling realistic Li^+ flux for high-energy lithium metal batteries. *Nat. Commun.* **2022**, *13*, 5431.

[34] Ji, H. X.; Zhao, X.; Qiao, Z. H.; Jung, J.; Zhu, Y. W.; Lu, Y. L.; Zhang, L. L.; Macdonald, A. H.; Ruoff, R. S. Capacitance of carbon-based electrical double-layer capacitors. *Nat. Commun.* **2014**, *5*, 3317.

Data availability

All data needed to support the conclusions in the paper are presented in the manuscript and the Electronic Supplementary Information. Additional data related to this paper may be requested from the corresponding author upon request.

Acknowledgements

The authors appreciate the financial support from Shanghai Jiao Tong University (No. WH220428007), the National Natural Science Foundation of China (Nos. 24Z990200631 and 25Z033004510), Shanghai Natural Science Foundation (Nos. 24ZR1434300 and 24ZR1440100), and China Postdoctoral Science Foundation (No. 2024M761937).

Author contributions

S. Q. Z., X. L. F. and T. D. conceived the idea. S. Q. Z. performed the electrochemical measurements and material characterization, analyzed the results, and wrote the manuscript. H. T. Z., J. Y. H., J. Z. W., L. L., L. C., R. H. L., and L. X. C. participated in the discussions. T. D. supervised all the studies and revised the manuscript.

Competing interests

The authors have no competing interests to declare that are relevant to the content of this article.

Use of AI statement

None.

Additional information

Supplementary Information The online version contains supplementary material available at https://doi.org/10.26599/CF.2026.9200068.